

Orbital structures in spinel vanadates AV_2O_4 ($A = \text{Fe, Mn}$)

Y. Nii,^{1,2} H. Sagayama,² T. Arima,^{1,2,3} S. Aoyagi,⁴ R. Sakai,⁵ S. Maki,⁵ E. Nishibori,⁵ H. Sawa,⁵ K. Sugimoto,⁶ H. Ohsumi,^{3,6} and M. Takata^{3,6}

¹*Institute of Multidisciplinary Research for Advanced Materials, Tohoku University, Sendai 980-8577, Japan*

²*Department of Advanced Materials Science, University of Tokyo, Kashiwa 277-8561, Japan*

³*RIKEN SPring-8 Center, Hyogo 679-5148, Japan*

⁴*Department of Information and Biological Science, Nagoya City University, Nagoya 467-8501, Japan*

⁵*Department of Applied Physics, Nagoya University, Nagoya 464-8603, Japan*

⁶*SPring-8/JASRI, Kouto, Sayo, Hyogo 679-5198, Japan*

(Received 25 June 2012; published 28 September 2012)

Spinel FeV_2O_4 exhibits successive structural phase transitions, reflecting the interplay between the Fe^{2+} ($3d^6$) and V^{3+} ($3d^2$) ions, both of which have orbital and spin degrees of freedom. The temperature-dependent orbital shapes of Fe^{2+} and V^{3+} were investigated by means of single-crystal structure analysis, and were compared with those in MnV_2O_4 , where only the V^{3+} ions are Jahn-Teller active. The highest-temperature transition from the cubic to the high-temperature tetragonal phase was driven by a ferroic Fe^{2+} $3z^2-r^2$ orbital order (OO). At 110 K, where the ferrimagnetic transition takes place, the magnetic order modified the orbital shape through intratomic spin-orbit coupling, causing an orthorhombic distortion. The V^{3+} orbital order (V-OO) contributed to the lowest temperature transition from the orthorhombic to the low-temperature tetragonal phase. The V-OO in FeV_2O_4 was qualitatively different from that in MnV_2O_4 . We propose that ferro-OO contains a complex orbital in FeV_2O_4 in contrast to the V-OO of real orbitals observed in MnV_2O_4 .

DOI: [10.1103/PhysRevB.86.125142](https://doi.org/10.1103/PhysRevB.86.125142)

PACS number(s): 75.25.Dk, 61.50.Ks, 71.70.Ej

I. INTRODUCTION

The orbital degree of freedom has attracted interest in modern condensed-matter physics, because various emergent phenomena arise through its coupling with spin, charge, and lattice degrees of freedom.¹ When the shape of the orbital is changed by an external stimulus, the magnetic, electric, elastic, and optical properties may also be altered. Spinel oxides with the general formula AB_2O_4 provide a fertile playground for studying the interplay between these degrees of freedom. In addition, magnetic spinels are one of the most representative geometrically frustrated systems, because the spinel B site forms a network of corner-sharing tetrahedra, referred to as a pyrochlore lattice.² Figure 1(a) shows the crystal structure of the AB_2O_4 spinel oxides. The A-site and B-site cations are tetrahedrally and octahedrally coordinated by oxygen ligands, respectively. In AV_2O_4 spinel vanadates, the V^{3+} ions selectively occupy the B sites and two $3d$ electrons are accommodated in the triply degenerate t_{2g} state. The orbital-related phenomena in this typical t_{2g} system have been thoroughly investigated in recent years.^{2–18} Several interactions, including the Kugel-Khomskii-type exchange interaction, relativistic spin-orbit (SO) coupling, and Jahn-Teller (JT) coupling, may compete with each other in spinel vanadates,^{3,4} giving rise to various V-orbital order (OO) patterns. For example, Tsunetsugu and Motome predicted that an OO with a propagation vector of $(0\ 0\ 2)$, known as an A-type OO, should arise from Kugel-Khomskii-type interaction,⁵ and Tchernyshyov proposed that a ferro (F)-OO should appear with a large relativistic SO coupling.⁴ Figure 1(c) shows a schematic phase diagram of MnV_2O_4 , where only the B-site V^{3+} (t_{2g}^2) ions are JT active. The ferrimagnetic transition of MnV_2O_4 occurs at $T_c = 56$ K, with the Mn^{2+} and V^{3+} spins aligned antiparallel to each other. The V-OO occurs at $T_s = 53$ K, and involves compressed tetragonal distortion ($c < a$).⁶

The spin configuration becomes noncollinear, and the V^{3+} moments are canted from the c axis by about 65° .⁷ Initially, the OO pattern of V^{3+} was proposed to be the A-type antiferro (AF)-OO,^{7,8} where one $3d$ electron occupies the xy orbital at every V site, and the other occupies the yz and zx orbitals alternately along the c axis.⁵ Subsequent theoretical research by Sarkar *et al.*⁹ and Chern *et al.*¹⁰ suggested that a large trigonal distortion of the VO_6 octahedra makes the orbital shapes more complicated. Accurate structural parameters for the low-temperature phase in MnV_2O_4 are essential for determining the exact orbital shapes.

The introduction of JT-active A-site ions in vanadium spinel AV_2O_4 should produce unusual physical properties arising from the competition or cooperation between the A and B sites. In FeV_2O_4 , the A-site Fe^{2+} with a high-spin d^6 ($S = 2$) configuration has twofold degeneracy in the lower-lying e orbital, in addition to threefold degeneracy at the V site [Fig. 1(a)]. These orbitals have smaller JT-coupling energies than the t_2 and e_g orbitals do, and thus the energy scales for several interactions are close to each other.³ This results in a highly degenerate energy manifold and in intriguing physical properties. Figure 1(b) shows a schematic illustration of the crystal structure of FeV_2O_4 as a function of temperature, and its successive structural phase transitions.¹¹ During cooling, a purely structural phase transition takes place at 140 K, from the cubic to the high-temperature (HT) tetragonal phase, where $c < a$. Collinear ferrimagnetic (FM) order emerges at 110 K, where the magnetic moments of the A-site Fe^{2+} and B-site V^{3+} align antiparallel to each other¹² and the crystal symmetry lowers from HT tetragonal to orthorhombic. The final structural transformation from orthorhombic to low-temperature (LT) tetragonal, where $c > a$ at ~ 70 K,¹³ accompanies another magnetic transition to a noncollinear configuration,¹² similar to that in MnV_2O_4 . The two tetragonal phases have

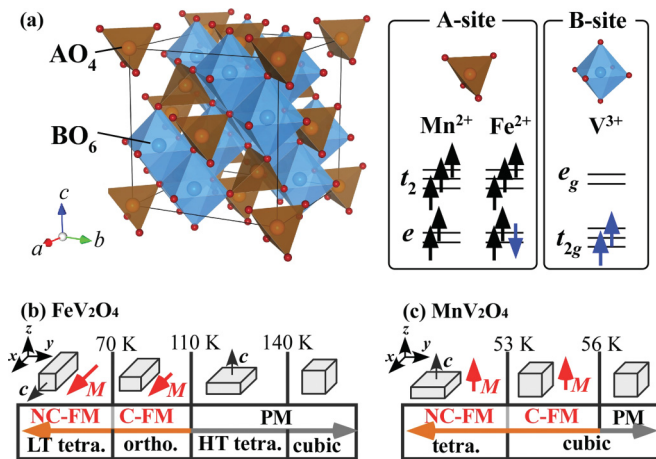


FIG. 1. (Color online) (a) Schematic illustration of the AB_2O_4 spinel oxides. FeV_2O_4 has orbital and spin degrees of freedom both at the A site (Fe^{2+}) and at the B site (V^{3+}). MnV_2O_4 has orbital-active ions at only the B-site V^{3+} . Schematic illustrations of the phase diagrams with crystallographic strain for (b) FeV_2O_4 and (c) MnV_2O_4 . The red arrows indicate the magnetization (M) direction. The phases are labeled paramagnetic (PM), collinear-ferrimagnetic (C-FM), and noncollinear-ferrimagnetic phase (NC-FM).

different macroscopic distortion, and the tetragonal c axes are perpendicular to each other in one domain.¹¹ Katsufuji *et al.*¹¹ have reported that the LT tetragonal phase below 70 K, where $c > a$, is unique because the constituent polyhedra (FeO_4 and VO_6) prefer the compressed tetragonal structure where $c < a$.^{14–17,19} This suggests that cooperation or competition between the Fe^{2+} and V^{3+} ions should be indispensable for generating a tetragonal structure where $c > a$. During the transition to the LT tetragonal phase, the V^{3+} moments are canted to form a noncollinear magnetic structure, where the moments form a 2-in 2-out spin configuration, similar to spin-ice systems in pyrochlore lattice in a strong magnetic field along the c axis.²⁰ Structural analyses by powder x-ray diffraction¹¹ and neutron diffraction¹² for examining the O-O bond lengths¹¹ and the O-Fe-O bond angles¹² in the FeO_4 tetrahedra showed that the orbital shape of Fe^{2+} changes from $3z^2-r^2$ type in the HT tetragonal phase to x^2-y^2 type in the LT tetragonal phase. In contrast, there is little information about V-OO. Sarkar and Saha-Dasgupta reported a first-principles calculation, which suggested that the V^{3+} orbitals are in the ferroic ($q = 0$) order with a commensurate modulation caused by the trigonal distortion of the VO_6 octahedra.²¹

In this paper we have investigated the orbital shapes of both Fe^{2+} and V^{3+} in FeV_2O_4 by means of single-crystal structure analysis using synchrotron x-ray diffraction, and compared them with those of MnV_2O_4 . There is usually some ambiguity in the structural parameters obtained from powder diffraction data. For example, it has been reported that for the V^{3+} orbital ordered phase in MnV_2O_4 , no change in reflection conditions across the phase transition was detected by powder x-ray diffraction,⁶ which is inconsistent with a single-crystal study that showed that some glide reflections are broken.⁸ The intensities of the $(h\ 0\ l)$ reflections with $h + l = 4n + 2$ are too weak to be observed in powder patterns. Therefore, we performed a single-crystal diffraction study to

investigate the crystallographic symmetries of FeV_2O_4 and MnV_2O_4 . To avoid the possible formation of twins below T_c , which could make the crystal structure analysis difficult, we used a crystal with a typical dimension of $\sim 20\ \mu\text{m}$, which generally consisted of a single domain in the tetragonal and orthorhombic phases. We examined the reflection conditions and carried out a single-crystal structure analysis in order to determine the space group and the crystallographic parameters precisely for each phase. In addition, a normal-mode analysis of the FeO_4 tetrahedra and the VO_6 octahedra was performed by using our experimental structural parameters. Assuming a strong electron-lattice coupling, the one-to-one correspondence between the orbital shape and atomic coordinates of oxygen ligands^{19,22,23} enabled us to perform a semiquantitative determination of the orbital states of Fe^{2+} and V^{3+} for FeV_2O_4 and MnV_2O_4 .

II. EXPERIMENT

Polycrystalline samples of FeV_2O_4 and MnV_2O_4 were prepared by a solid-state reaction. Stoichiometric amounts of Fe, Fe_2O_3 , and V_2O_3 for FeV_2O_4 , and MnO and V_2O_3 for MnV_2O_4 were mixed and pressed into bars. The FeV_2O_4 bar was heated at 1273 K for 20 h in an evacuated silica tube, whereas the MnV_2O_4 bar was heated at 1473 K for 12 h in an Ar/ H_2 gas flow. By using these polycrystalline bars, single crystals of FeV_2O_4 and MnV_2O_4 were grown by the floating-zone method in an Ar gas flow at a growth rate of $\sim 3.0\ \text{mm/h}$. The maximum dimension of the FeV_2O_4 crystals was about 2 mm. Conventional x-ray diffraction measurements showed that the samples consisted of a single spinel phase. The magnetization in FeV_2O_4 was measured with a superconducting quantum interference device magnetometer. The reflection conditions for each phase of FeV_2O_4 and MnV_2O_4 were checked by using relatively large crystals with a typical dimension of about $100\ \mu\text{m}$. In contrast, small crystals with a typical dimension (x) of about $20\ \mu\text{m}$, such that $\mu x \approx 0.03$, were used for the single-crystal structure analysis. Here μ denotes the absorption coefficient. The small crystals also possessed a large imbalance in the tetragonal or orthorhombic domains. The MnV_2O_4 sample was cooled from room temperature to 20 K in a magnetic field by placing a permanent magnet near the sample. To collect intensity data with sufficient statistics from the tiny crystals, we used a synchrotron x-ray diffractometer on beamline BL02B1 at SPring-8, Japan. The diffracted x rays were detected by a large cylindrical imaging plate (IP). The wavelengths of incident x rays were $0.3600\ \text{\AA}$ for FeV_2O_4 and $0.35438\ \text{\AA}$ for MnV_2O_4 . The crystal structure analysis was performed by using CrystalStructure (Rigaku Corp. and MSC). The deviations of g factors from ideal values were within 3% in the cubic phases. Figures 2(a) and 2(b) show three-dimensional plots of the IP images around the $(0\ 0\ 8)_c$ and $(4\ 0\ 0)_c$ reflections from a $20\ \mu\text{m}$ crystal of FeV_2O_4 at 40 K; the suffix c indicates the index in the face-centered tetragonal setting. The peak-height ratios were 82:12:6 for $\{0\ 0\ 8\}_c$ and 98:1:1 for $\{4\ 0\ 0\}_c$, which showed that one domain state was dominant in the LT tetragonal phase in FeV_2O_4 . In addition, the strongest peak was well separated from the other two minor peaks. In the HT tetragonal and orthorhombic phases in FeV_2O_4 and in the

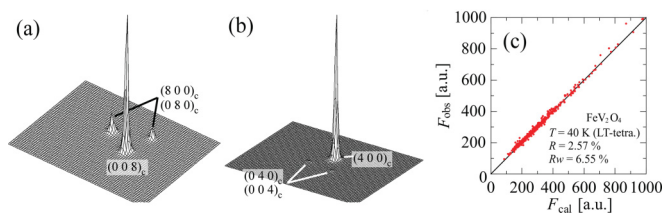


FIG. 2. (Color online) The 3D plots of IP images around (a) the $(0\ 0\ 8)_c$ and (b) the $(4\ 0\ 0)_c$ reflections for a $20\ \mu\text{m}$ crystal at 40 K (LT tetragonal phase) in FeV_2O_4 . The reflections were indexed in the cubic setting. The peak height ratios were 82:12:6 for $\{8\ 0\ 0\}_c$ and 98:1:1 for $\{4\ 0\ 0\}_c$, showing that an almost twin-free state was achieved. In addition, the strongest peak was well separated from the other two minor peaks, which arose from the second and third domains. The crystal structure analysis was carried out by masking the most relevant peak. (c) Comparison of the calculated (F_{cal}) and the experimental (F_{obs}) structure factors for FeV_2O_4 at 40 K (LT tetragonal).

tetragonal phase in MnV_2O_4 , one dominant peak and separated twin peaks with much lower intensities were observed. The crystal structure analysis was successfully carried out for each phase in FeV_2O_4 and MnV_2O_4 by masking the most relevant peaks. Figure 2(c) shows a comparison between the calculated (F_{cal}) and observed (F_{obs}) structure factors for FeV_2O_4 at 40 K. The crystallographic parameters are summarized in Tables I to IV. Figure 1(b) shows that the fourfold axis in the HT tetragonal phase was perpendicular to that in the LT tetragonal phase. The x , y , and z axes are defined as shown in Fig. 1(b).

III. RESULTS

Figure 3 shows temperature dependence of the magnetization and lattice constants of FeV_2O_4 . The lattice constant a for each body-centered tetragonal phase was multiplied by $\sqrt{2}$ for comparison. During cooling, successive structural phase transitions were observed from the cubic to the HT tetragonal phase ($c < a$) at 140 K, from the HT tetragonal to the orthorhombic phase at 110 K, and from the orthorhombic to the LT tetragonal phase ($c > a$) at 65 K. The structural transition at 110 K accompanies the onset of spontaneous magnetization. These results agree well with previously reported transitions, although we did not observe a further transition to another orthorhombic phase at 35 K.¹¹

Determining the crystallographic symmetry is essential for revealing the OO pattern. Figures 4(a) and 4(b) show the typical IP images of the cubic and tetragonal phases in FeV_2O_4 and MnV_2O_4 . The $(4\ 0\ -2)_c$ reflection was observed in the tetragonal phase of MnV_2O_4 [Fig. 4(b)]. Figure 4(c) shows the temperature dependence of the integrated intensity of the $(4\ 0\ -2)_c$ reflection for MnV_2O_4 . The reflection suddenly appears below T_s , which is consistent with previous results.⁸ The other reflection condition $k + l = 4n + 2$ for $(0\ k\ l)_c$ was also relaxed in the tetragonal phase in MnV_2O_4 (not shown). The presence of $(0\ k\ l)_c$ and $(h\ 0\ l)_c$ reflections with $k + l = 4n + 2$ and $h + l = 4n + 2$ indicates the d -glide planes normal to the a and b axes were violated, because the symmetry was lowered from $I4_1/amd$ to $I4_1/a$. In contrast, in FeV_2O_4 the $(0\ -4\ 6)_c$ reflection remained forbidden in the LT tetragonal phase [Fig. 4(a)]. We did not detect any $(h\ 0\ l)_c$ or $(hk\ 0)_c$ reflections with $h + l = 4n + 2$ or $h + k = 4n + 2$. These results indicate that FeV_2O_4 maintained the $I4_1/amd$ symmetry with three d -glide planes normal to the a , b , and c axes. The differences between FeV_2O_4 and MnV_2O_4 can be attributed to the different V^{3+} OO patterns; this is discussed in detail later.

By determining the reflection conditions in a similar manner, the crystallographic symmetries were found to be $Fd-3m$, $I4_1/amd$, and $Fddd$ for the cubic, tetragonal, and orthorhombic phases in FeV_2O_4 , and $Fd-3m$ and $I4_1/a$ for the cubic and tetragonal phases in MnV_2O_4 , respectively. A structural analysis was performed based on the space group, and the parameters are listed in Tables I to VI. To consider the orbital states of the V^{3+} ions, we analyzed the distortion of the VO_6 octahedra in terms of normal modes. In an octahedrally coordinated $\text{V}^{3+}(t_{2g}^2)$ system, the orbital degree of freedom can interact with the E_g (Q_2 , Q_3) and T_{2g} (Q_4 , Q_5 , Q_6) modes²⁴ shown in Fig. 5(a). The five modes can be expressed as

$$\begin{aligned} Q_2 &= (X_1 - Y_2 - X_3 + Y_5)/2, \\ Q_3 &= (-X_1 - Y_2 + 2Z_3 + X_4 + Y_5 - 2Z_6)/2\sqrt{2}, \\ Q_4 &= (Z_2 + Y_3 - Z_5 - Y_6)/2, \\ Q_5 &= (Z_1 + X_3 - Z_4 - X_6)/2, \\ Q_6 &= (Y_1 + X_2 - Y_4 - X_5)/2, \end{aligned} \quad (1)$$

where U_i ($U = X, Y, Z$, and $i = 1$ to 6) represents the displacement for the i th oxygen atom in the U direction. The Q_2 and Q_3 modes are orthorhombic and tetragonal distortions, respectively, and the Q_4 - Q_6 modes correspond to the deviation

TABLE I. Structure parameters for cubic FeV_2O_4 at 150 K with $Fd-3m$ symmetry. The lattice parameter is $a = 8.43920(10)$ (\AA), the volume is $V = 601.041(12)$ (\AA^3). The reliability factors are $R = 1.88\%$, $R_w = 2.76\%$, and the goodness of fit (GOF) indicator is $\text{GOF} = 1.142$.

Site	x	y	z	B (\AA^2)	g
Fe	$8a$	0.125	0.125	0.423(2)	1.015(7)
V	$16d$	0.5	0.5	0.306(1)	1.022(8)
O	$32e$	0.73882(7)	0.73882(7)	0.406(5)	1
	U_{11}	U_{22}	U_{33}	U_{12}	U_{13}
Fe	0.00536(5)	0.00536(5)	0.00536(5)	0.0000	0.0000
V	0.00388(4)	0.00388(4)	0.00388(4)	-0.00007(4)	-0.00007(4)
O	0.00514(15)	0.00514(15)	0.00514(15)	-0.00046(10)	-0.00046(10)

TABLE II. Structure parameters for tetragonal FeV_2O_4 at 120 K with $I4_1/amd$ symmetry. The lattice parameters are $a = 5.99723(16)$ (Å) and $c = 8.35450(10)$ (Å), and the volume is $V = 300.484(12)$ (Å³). The reliability factors are $R = 2.68\%$, $R_w = 7.60\%$, and the goodness of fit (GOF) indicator is $\text{GOF} = 3.555$.

	Site	x	y	z	B (Å ²)	g
Fe	4b	0.5	0.25	0.625	0.381(5)	1.03(2)
V	8c	0.25	0.75	0.75	0.285(3)	1.05(2)
O	16h	0.5	0.97497(18)	0.75879(14)	0.372(13)	1
	U_{11}	U_{22}	U_{33}	U_{12}	U_{13}	U_{23}
Fe	0.00467(12)	0.00467(12)	0.00512(14)	0.000	0.000	0.000
V	0.00358(9)	0.00378(10)	0.00347(8)	0.000	-0.00004(6)	0.000
O	0.0053(3)	0.0044(3)	0.0044(3)	0.000	0.000	0.00057(17)

of the O-V-O angle from $\pi/2$. The linear combination of the T_{2g} (Q_4, Q_5, Q_6) modes produces the trigonal distortion Q_t as expressed by $Q_t = (Q_4 + Q_5 + Q_6)/\sqrt{3}$, which corresponds to the elongation or compression along one of the four $\langle 111 \rangle_c$ axes. Figures 5(b) and 5(c) show the temperature dependence of the E_g (Q_2, Q_3) modes and the trigonal distortion (Q_t) for FeV_2O_4 . It should be noted that the B site in the spinel structure is coordinated by a trigonally elongated octahedron. At the lowest temperature there was a clear increase in the Q_2 (~ 0.02 Å) and Q_3 (~ 0.01 Å) modes. This indicates that a substantial V-OO emerged in only the LT tetragonal phase. In contrast, the trigonal deformation showed little temperature dependence (less than ~ 0.005 Å), and did not affect V-OO. In addition, the Q_2 and Q_3 modes of MnV_2O_4 developed below the structural transition, whereas Q_t remained unaltered across the transition [Figs. 5(d) and 5(e)], suggesting that the V-OO in MnV_2O_4 should be also triggered by the coupling to the Q_2 and Q_3 modes. The Q_t mode for MnV_2O_4 was ~ 0.05 Å larger than that of FeV_2O_4 . Although these large trigonal distortions did modify the t_{2g} orbital shapes,^{9,10} Q_t did not play the most important role in the orbital and structure phase transitions. Therefore we focused on the variation of the E_g (Q_2, Q_3)-mode distortion.

To determine the orbital states of Fe^{2+} , a normal-mode analysis of the FeO_4 tetrahedron was also carried out. The distortion of an FeO_4 tetrahedron can be represented just by the symmetric Q_1 (breathing) and two-dimensional Q_2 - Q_3 modes. Figures 6(a) and 6(b) represent the local distortion of the FeO_4 tetrahedron and the VO_6 octahedron for FeV_2O_4

in the Q_2 - Q_3 plane, where the angle θ from the Q_3 axis reflects the anisotropy of the orbital. In Fig. 6(a) the shape of the e orbital on Fe^{2+} coupled to each local mode is also shown. Figure 6(c) shows the temperature dependence of the global distortion in the u_2 - u_3 plane, calculated from the temperature dependence of the lattice constant shown in Fig. 3(b). Here the global distortions u_2 and u_3 correspond to the local modes Q_2 and Q_3 , respectively. During cooling, the global structure continuously changed in the u_2 - u_3 plane from cubic to the HT tetragonal phase where $c < a$ ($\theta = \pi$), and then through the orthorhombic ($\pi > \theta > 2\pi/3$) to the LT tetragonal phase where $c > a$ ($\theta = 2\pi/3$). In one domain, the principle axes (c axis) of these two tetragonal phases were perpendicular to each other. The temperature dependence of the local FeO_4 distortion [Fig. 6(a)] was qualitatively similar to that of the global distortion. In the paramagnetic tetragonal phase at 120 K, all the FeO_4 tetrahedra were tetragonally distorted in a compressed fashion. This corresponds to the ferroic occupation of the $3z^2-r^2$ orbital by a minority-spin electron at the Fe^{2+} site. At 90 K below the ferrimagnetic transition, the orthorhombic distortion appeared, which was a mixture of the compressed ($\theta = \pi$) and elongated ($\theta = 2\pi/3$) tetragonal distortion of the FeO_4 tetrahedron. This means that the minority-spin electron occupied the orbital expressed by a linear combination of the corresponding $3z^2-r^2$ ($\theta = \pi$) and y^2-z^2 ($\theta = 2\pi/3$) orbitals. At 40 K, the FeO_4 distortion became tetragonal again, although it was elongated along the x direction ($\theta = 2\pi/3$), indicating that the Fe^{2+} orbital state transformed perfectly from $3z^2-r^2$ to y^2-z^2 . However, the local

TABLE III. Structure parameters for orthorhombic FeV_2O_4 at 90 K with $Fddd$ symmetry. The lattice parameters are $a = 8.52450(10)$ (Å) and $b = 8.3229(2)$ (Å), $c = 8.4612(5)$ (Å), and the volume is $V = 600.31(4)$ (Å³). The reliability factors are $R = 3.26\%$, $R_w = 8.54\%$, and the goodness of fit (GOF) indicator is $\text{GOF} = 3.119$.

	Site	x	y	z	B (Å ²)	g
Fe	8a	0.125	0.125	0.125	0.306(4)	0.98(2)
V	16d	0	0.25	0.75	0.223(2)	1.00(2)
O	32h	0.98640(10)	0.25792(13)	0.98822(11)	0.343(11)	1
	U_{11}	U_{22}	U_{33}	U_{12}	U_{13}	U_{23}
Fe	0.00298(11)	0.00434(12)	0.00430(12)	0.0000	0.0000	0.0000
V	0.00241(6)	0.00282(7)	0.00324(7)	-0.00002(5)	0.00011(5)	-0.00001(5)
O	0.0039(2)	0.0042(3)	0.0050(2)	0.00043(14)	-0.00021(13)	0.00031(16)

TABLE IV. Structure parameters for tetragonal FeV_2O_4 at 40 K with $I4_1/amd$ symmetry. The lattice parameters are $a = 5.9307(3)$ (Å) and $c = 8.5321(2)$ (Å), and the volume is $V = 300.10(2)$ (Å³). The reliability factors are $R = 2.57\%$, $R_w = 6.55\%$, and the goodness of fit (GOF) indicator is $\text{GOF} = 1.381$.

	Site	x	y	z	B (Å ²)	g
Fe	4b	0.5	0.25	0.125	0.222(3)	0.992(16)
V	8c	0.25	0.75	0.25	0.171(2)	1.00(2)
O	16h	0.5	0.98171(17)	0.26522(10)	0.290(10)	1
	U_{11}	U_{22}	U_{33}	U_{12}	U_{13}	U_{23}
Fe	0.00291(9)	0.00291(9)	0.00262(11)	0.0000	0.0000	0.0000
V	0.00210(7)	0.00209(8)	0.00229(7)	0.0000	-0.00019(5)	0.0000
O	0.0046(3)	0.0031(2)	0.0034(2)	0.0000	0.0000	0.00039(14)

distortion of the VO_6 octahedron below 40 K was compressed along the x direction ($\theta = 5\pi/3$) [Fig. 6(b)]. The pattern of the VO_6 distortion was also ferroic in the Q_2 - Q_3 plane. The tetragonal distortion of VO_6 was the opposite of both the local FeO_4 tetrahedron and the global crystallographic distortion.

A mode analysis of the VO_6 distortion in MnV_2O_4 was also carried out. Figure 7 shows the Q_2 - Q_3 plot of the VO_6 distortion for MnV_2O_4 in the cubic (80 K) and tetragonal (20 K) phases. To our knowledge, this is the first time the quantitative distortion of the VO_6 octahedron in MnV_2O_4 has been reported. Unlike in FeV_2O_4 , in MnV_2O_4 there were two VO_6 sites at 20 K, which yielded elongation strain of about 0.04 Å in the approximate direction of the x ($\theta \sim 2\pi/3$) or y ($\theta \sim 4\pi/3$) axis. These two VO_6 sites were alternately arranged along the z axis [Fig. 7(a)]. The two V sites were crystallographically equivalent, because they were connected by a 4_1 symmetry operation. The average distortion of the two types of VO_6 octahedral sites can be expressed as $\theta = \pi$, which is consistent with the global distortion in MnV_2O_4 , where the tetragonal structure is compressed along the z axis.⁶ Another striking difference in the VO_6 distortion between FeV_2O_4 and MnV_2O_4 was the sign of the local VO_6 distortion. The VO_6 octahedra in FeV_2O_4 were compressed, whereas those in MnV_2O_4 were elongated.

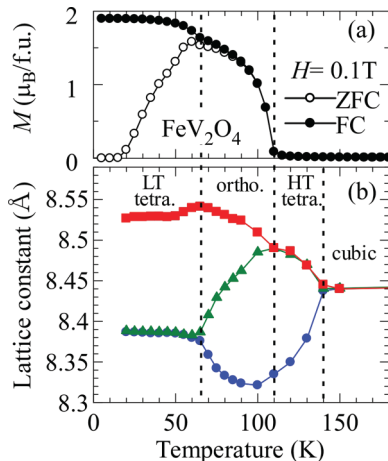


FIG. 3. (Color online) (a) Temperature dependence of the magnetization (M) and (b) lattice constants for FeV_2O_4 .

IV. DISCUSSION

A. Successive phase transitions in FeV_2O_4

The first phase transition from the cubic to the HT tetragonal phase at 140 K where $c < a$ in FeV_2O_4 was attributed to the cooperative JT transition of FeO_4 . Öpik and Pryce²⁴ have reported that the elastic energy of the third-order term, expressed as $V = A_3 Q^3 \cos(3\theta)$, lifts the infinite degeneracy with respect to θ in the Q_2 - Q_3 plane, where A_3 is the third-order elastic constant, and $Q = (Q_2^2 + Q_3^2)^{1/2}$. For the tetrahedral sites, A_3 was positive, and hence the elastic anharmonicity stabilized the compressed tetragonal distortion of $\theta = \pi/3, \pi$, and $5\pi/3$. The ferroic interactions among each isolated FeO_4 tetrahedron resulted in a cooperative JT distortion, which should produce a $3z^2 - r^2$ F -OO with a $-Q_3$ distortion ($\theta = \pi$). This was consistent with the data at 120 K. Therefore, the first transition was purely driven by Fe-OO. However, the second-highest phase transition at 110 K was spin driven; the SO interaction at the Fe^{2+} site should trigger the structural change. There are no orbital angular momentum matrix elements for e orbital states. However, taking into account the virtual excitation to the empty t_2 states as a second-order perturbation, the orbital angular momentum at the Fe^{2+} site can be partially recovered, which leads to a nonzero SO interaction. This SO interaction can be expressed

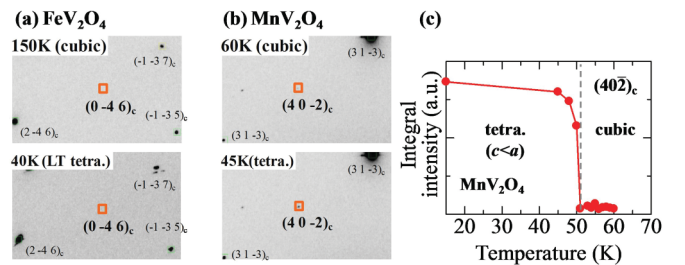


FIG. 4. (Color online) IP images for the cubic and tetragonal phases in (a) FeV_2O_4 and (b) MnV_2O_4 . (c) Temperature dependence of the integral intensity of the $(40-2)$ forbidden reflections. In MnV_2O_4 an abrupt increase in intensity was observed below T_s , which indicates the breaking of the d -glide symmetry, whereas there was no change in the intensity for the tetragonal phase in FeV_2O_4 . This indicates that the space group of the tetragonal phase in MnV_2O_4 should be $I4_1/a$, whereas FeV_2O_4 maintains the highest symmetry in the tetragonally distorted spinel structure $I4_1/amd$.

TABLE V. Structure parameters for cubic MnV_2O_4 at 80 K with $Fd-3m$ symmetry. The lattice parameters is $a = 8.5325(2)$, and the volume is $V = 621.20(3)$ (\AA^3). The reliability factors are $R = 1.26\%$, $R_w = 3.05\%$, and the goodness of fit (GOF) indicator is $\text{GOF} = 1.112$.

	Site	x	y	z	B (\AA^2)	g
Mn	$8a$	0.125	0.125	0.125	0.209(2)	1.022(7)
V	$16d$	0.5	0.5	0.5	0.1753(12)	1.015(7)
O	$32e$	0.73715(5)	0.73715(5)	0.73715(5)	0.290(4)	1
	U_{11}	U_{22}	U_{33}	U_{12}	U_{13}	U_{23}
Mn	0.00265(6)	0.00265(6)	0.00265(6)	0.0000	0.0000	0.0000
V	0.00222(3)	0.00222(3)	0.00222(3)	-0.00010(3)	-0.00010(3)	-0.00010(3)
O	0.00367(12)	0.00367(12)	0.00367(12)	-0.00036(7)	-0.00036(7)	-0.00036(7)

as $H_{\text{SO}} = B/6[(3S_z^2 - S^2)\tau_z - \sqrt{3}(S_x^2 - S_y^2)\tau_x]$,¹⁹ where τ_z and τ_x are pseudospin operators representing the e orbital, and B (>0) is the energy difference between the $3z^2-r^2$ and x^2-y^2 orbitals, which are eigenstates of the τ_z operator. For instance, under the second-order perturbations of the SO interaction, the x^2-y^2 ($\theta = 0$), y^2-z^2 ($\theta = 2\pi/3$), and z^2-x^2 ($\theta = 4\pi/3$) orbitals are energetically favorable when the Fe^{2+} spin is aligned along the z , x , and y axes, respectively. Thus, the orbital shape of Fe^{2+} could be modulated through the SO interaction, once the magnetic order sets in at 110 K. The SO interaction would mean that the Fe^{2+} moment should lie in the x - y plane in the HT tetragonal phase with the $3z^2-r^2$ F -OO. For example, when the Fe^{2+} spin moments are aligned in the x direction below $T_c = 110$ K, the y^2-z^2 orbital would be stabilized by the SO interaction, resulting in a mixture of the $3z^2-r^2$ and y^2-z^2 orbital. Consequently, a positive Q_2 distortion should arise through the electron-lattice coupling [Fig. 6(a)], lowering the global crystallographic symmetry to an orthorhombic symmetry [Fig. 6(c)]. The global structure below T_c undergoes elongation along the magnetization direction which is parallel to the Fe^{2+} spin direction [Fig. 1(b)].^{11,12} This is consistent with the discussion about the change in orbital shapes. The scenario can elucidate the first two phase transitions in FeV_2O_4 during cooling. It is similar to that of FeCr_2O_4 with a JT-active ion at only the Fe^{2+} site, which also undergoes successive structural phase transitions from cubic, to tetragonal, and then to orthorhombic as the temperature decreases.¹⁹ At the transition from the tetragonal to the orthorhombic phase, the ferrimagnetic order appears in both FeCr_2O_4 and FeV_2O_4 . Therefore, the first two phase transitions could be attributed

to only the Fe site. However, there are critical differences between FeV_2O_4 and FeCr_2O_4 ; in the orthorhombic distortion, the deviation angle $\Delta\theta$ from $\theta = \pi$ is small for FeCr_2O_4 ($\Delta\theta \sim 7^\circ$)¹⁹ compared with that of FeV_2O_4 ($\Delta\theta$ of up to $\pi/3$). As a result, the lowest transition to the LT tetragonal phase was observed in FeV_2O_4 , but not in FeCr_2O_4 . The effect of the other JT-active ion V^{3+} may be necessary for the phase transition from the orthorhombic to the LT tetragonal phase to occur in FeV_2O_4 . The distortion of VO_6 observed at 40 K indicates that the lowest temperature transition to the LT tetragonal phase originated from the V-OO. Compression along the x direction should lift the t_{2g} degeneracy to a lower singlet (yz) and higher doublet (xy , zx) manifold, where the second electron still has an orbital degeneracy in the doublet. If the linear combination of these orbitals has a real coefficient, such as $1/\sqrt{2}(xy + zx)$, the orbitals can interact with only the Q_4 mode through orbital-lattice coupling. Thus, the real $1/\sqrt{2}(xy + zx)$ orbital cannot induce any E_g (Q_2 , Q_3) distortion, and it can couple to only the T_{2g} (Q_4 , Q_5 , Q_6) distortion. To account for the Q_2 - Q_3 distortion that we observed, a complex orbital, such as $1/\sqrt{2}(xy + izx)$, must be considered. If two electrons at the V site occupied the yz and $1/\sqrt{2}(xy + izx)$ orbitals, the VO_6 octahedron would be compressed along the x direction [Fig. 6(b)]. This suggests that the V-OO in the LT tetragonal phase is the F -OO with the complex orbital, where two V^{3+} electrons occupy the yz and the $1/\sqrt{2}(xy + izx)$ orbitals. This F -OO pattern was first proposed by Tchernyshyov⁴ for vanadium spinels with non-magnetic divalent A-site ions (Zn, Cd, Mg), considering the

TABLE VI. Structure parameters for tetragonal MnV_2O_4 at 20 K with $I4_1/a$ symmetry. The lattice parameters are $a = 6.05170(10)$ (\AA) and $c = 8.4639(3)$ (\AA), and the volume is $V = 309.974(13)$ (\AA^3). The reliability factors are $R = 1.79\%$, $R_w = 4.54\%$, and the goodness of fit (GOF) indicator is $\text{GOF} = 1.425$.

	Site	x	y	z	B (\AA^2)	g
Mn	$4a$	0	0.75	0.875	0.1790(17)	1.000(8)
V	$8d$	0.25	0.25	0.75	0.1526(11)	0.994(8)
O	$16f$	0.99669(10)	0.47426(7)	0.73747(5)	0.279(4)	1
	U_{11}	U_{22}	U_{33}	U_{12}	U_{13}	U_{23}
Mn	0.00233(4)	0.00233(4)	0.00214(5)	0.0000	0.0000	0.0000
V	0.00197(3)	0.00205(3)	0.00178(3)	0.00002(2)	-0.00014(2)	0.00001(2)
O	0.00426(12)	0.00320(11)	0.00315(12)	-0.00004(8)	0.00001(9)	-0.00036(6)

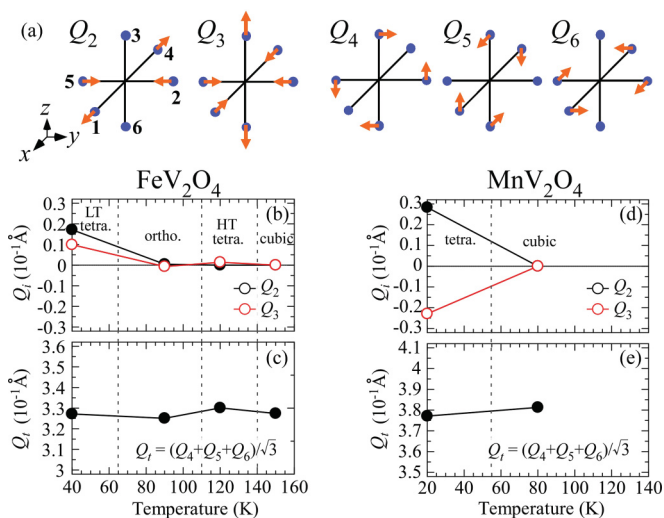


FIG. 5. (Color online) (a) Schematic illustration of the Q_2 and Q_3 (E_g), and the Q_4 , Q_5 , and Q_6 (T_{2g}) normal modes of an octahedron. Q_2 and Q_3 correspond to the orthorhombic and tetragonal distortion, respectively. The average of Q_4 , Q_5 , and Q_6 is the trigonal distortion $\pm Q_t$, which corresponds to elongation or compression along the $\langle 111 \rangle$ direction. The temperature dependence of each of the modes (Q_2 , Q_3 , Q_t) is shown for (b), (c) FeV_2O_4 , and (d), (e) MnV_2O_4 .

predominant SO interaction with the perturbed JT coupling. The model satisfies both the crystallographic symmetry of the $I4_1/amd$ and the compressed VO_6 octahedra in FeV_2O_4 . The F -OO model is significant because of the unquenched orbital angular momentum ($L_z = \pm 1$) of V^{3+} , which results from the wave function with the complex coefficient. Here the orbital polarization L_z is induced by the $yz \pm izx$ orbital, where the fourfold axis is taken along the z direction, although this is different from our indexing, where the orbital angular momentum arises along the x direction, because of the $xy + izx$ orbital. In view of the SO interaction, the total magnetic moment of V^{3+} should be dramatically reduced by the unquenched L ($\sim 1 \mu_B$) in the opposite direction to the spin component ($\sim 2 \mu_B$), where a magnetic moment of $\sim 1 \mu_B$ is anticipated. Strictly speaking, the trigonal distortion of VO_6 should modify the F -OO pattern. The yz and $1/\sqrt{2}(xy + izx)$ orbitals would be rotated to produce an orbital modulation along the $\langle 110 \rangle$ chains.^{9,10} Accordingly, the orbital angular momentum L would also be canted from the x axis toward the local trigonal axis, in the $\langle 111 \rangle_c$ direction, which would

link the spin moment canting in the $\langle 111 \rangle_c$ direction via SO coupling. This scenario requires a large reduction in the V^{3+} magnetic moments, and the noncoplanar spin configuration in the pyrochlore lattice similar to the 2-in 2-out spin structure. A recent neutron scattering study¹² reported a significant decrease in the V^{3+} magnetic moments ($\sim 0.8 \mu_B \ll 2.0 \mu_B$), and spin canting against the c axis ($\sim 55^\circ$) at the transition to the LT tetragonal phase. The V^{3+} moment was aligned to the center of the V_4 tetrahedron, characterized by the 2-in 2-out structure. These results strongly suggest the presence of unquenched orbital angular momentum in the LT tetragonal phase, and are consistent with our explanation. There are also some apparently contradictory studies. A recent XMCD experiment suggests a quenched orbital moment for the V^{3+} ion.²⁵ However the experiment was performed above 80 K, where complex-OO is not considered to be formed. In addition, a first-principles calculation suggested that the orbital pattern of V^{3+} in the LT tetragonal phase consists of a real orbital with an orbital moment of only 0.09 to 0.1 μ_B , even when the SO interaction is taken into account.²² The discrepancy may be caused by the use of the collinear ferrimagnetic structure in the calculation for the LT tetragonal phase. The formation of this unique complex orbital state in FeV_2O_4 may originate from the corner sharing of the FeO_4 tetrahedron and the VO_6 octahedron.²³ An effective interorbital interaction between the corner-sharing FeO_4 and VO_6 could be antiferroic through oxygen displacement. The elongation of an FeO_4 tetrahedron would compress the adjacent VO_6 octahedron, and lead to the formation of the complex orbital state at the V site.

B. Orbital order in MnV_2O_4

The VO_6 octahedra in MnV_2O_4 were elongated along the x or y axis, and stacked along the z axis (Fig. 7). Taking into account the electron-lattice coupling at the sites with $\theta \approx 2\pi/3$, where the VO_6 octahedron elongated approximately in the x direction, two electrons should occupy the xy and zx orbitals. In contrast, at the site where $\theta \sim 4\pi/3$, the xy and zy orbitals should be occupied, because of the elongation approximately in the y direction. This orbital pattern is identical to the A -type AF -OO proposed by Tsunetsugu and Motome,⁵ where one electron occupies the xy orbital at every V site, and the other electron alternately occupies the yz and zx orbitals. They proposed that the A -type AF -OO pattern should appear when the Kugel-Khomskii-type exchange interaction

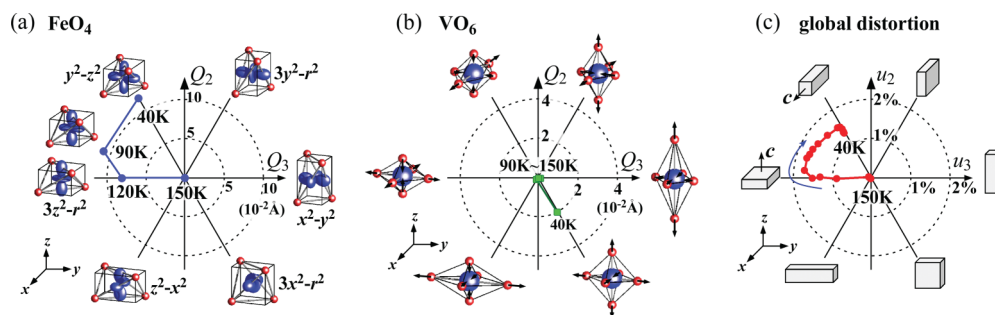


FIG. 6. (Color online) Q_2 - Q_3 mode analyses of (a) an FeO_4 tetrahedron and (b) a VO_6 octahedron. (c) The u_2 - u_3 plot of the global distortion for FeV_2O_4 . The u_2 - u_3 values were calculated from the lattice constants.

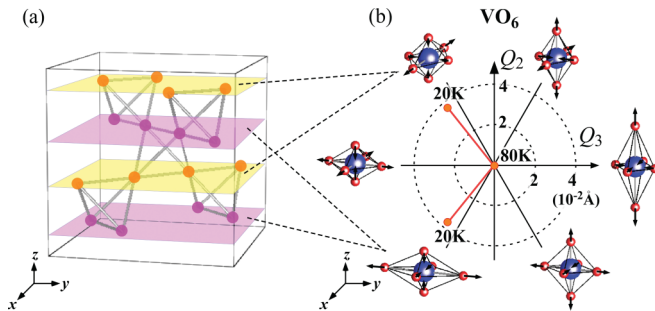


FIG. 7. (Color online) (a) Schematic illustration of the V-site pyrochlore lattice. (b) Distortion of the VO_6 octahedron for MnV_2O_4 in the Q_2 - Q_3 plane. For the tetragonal phase where $c < a$ (20 K) there were two sites with different local distortions, which alternately stack along the c axis (shown in purple and yellow) in (a).

is dominant, which is associated with the JT coupling.⁵ The observed VO_6 distortion is also energetically favorable in relation to the JT energy, because the energy levels of the two t_{2g} electrons are stabilized by the elongated tetragonal distortion along the x or y direction. The large elongation along the trigonal axis in MnV_2O_4 [Fig. 5(e)] would modify this simple orbital order pattern, as suggested by Sarkar *et al.*⁹ and Chern *et al.*¹⁰

V. CONCLUSIONS

In summary, we have performed a single-crystal synchrotron x-ray diffraction structural analysis of FeV_2O_4 , which has JT-active ions both at the A-site Fe^{2+} and the B-site V^{3+} , and compared it with MnV_2O_4 , in which only the V^{3+} ions are JT active. We determined the orbital states of Fe^{2+} and V^{3+} in each phase in FeV_2O_4 and MnV_2O_4 through normal-mode (Q_2 , Q_3) analysis of the FeO_4 tetrahedra and the VO_6 octahedra under the assumption of strong electron-lattice coupling. The successive structural phase transitions in FeV_2O_4 originated from the Fe^{2+} orbital order and its modulation through the SO coupling, and from the V^{3+} orbital order. The pattern of the V-OO of FeV_2O_4 was qualitatively different from that of MnV_2O_4 . The V-OO in FeV_2O_4 was an F -OO with the complex orbital characterized by the unquenched orbital angular momentum, whereas an AF -OO with real orbitals was realized in MnV_2O_4 .

ACKNOWLEDGMENTS

This work was partly supported by the Funding Program for World Leading Innovative R&D on Science and Technology (FIRST) on “Quantum Science on Strong Correlation” from JSPS, and by a Grant-in-Aid for Scientific Research from MEXT (No. 19052001). Y.N. was supported by a Grant-in-Aid for JSPS Fellows (Grant No. 234410) from JSPS.

¹Y. Tokura and N. Nagaosa, *Science* **288**, 462 (2000).

²S.-H. Lee, H. Takagi, D. Louca, M. Matsuda, S. Ji, H. Ueda, Y. Ueda, T. Katsufuji, J.-H. Chung, S. Park, S.-W. Cheong, and C. Broholm, *J. Phys. Soc. Jpn.* **79**, 011004 (2010).

³Y. Motome and H. Tsunetsugu, *Prog. Theor. Phys. Suppl. No.* **160**, 203 (2005).

⁴O. Tchernyshyov, *Phys. Rev. Lett.* **93**, 157206 (2004).

⁵H. Tsunetsugu and Y. Motome, *Phys. Rev. B* **68**, 060405(R) (2003).

⁶K. Adachi, T. Suzuki, K. Kato, K. Osaka, M. Takata, and T. Katsufuji, *Phys. Rev. Lett.* **95**, 197202 (2005).

⁷V. O. Garlea, R. Jin, D. Mandrus, B. Roessli, Q. Huang, M. Miller, A. J. Schultz, and S. E. Nagler, *Phys. Rev. Lett.* **100**, 066404 (2008).

⁸T. Suzuki, M. Katsumura, K. Taniguchi, T. Arima, and T. Katsufuji, *Phys. Rev. Lett.* **98**, 127203 (2007).

⁹S. Sarkar, T. Maitra, R. Valentí, and T. Saha-Dasgupta, *Phys. Rev. Lett.* **102**, 216405 (2009).

¹⁰G.-W. Chern, N. Perkins, and Z. Hao, *Phys. Rev. B* **81**, 125127 (2010).

¹¹T. Katsufuji, T. Suzuki, H. Takei, M. Shingu, K. Kato, K. Osaka, M. Takata, H. Sagayama, and T. Arima, *J. Phys. Soc. Jpn.* **77**, 053708 (2008).

¹²G. J. MacDougall, V. O. Garlea, A. A. Aczel, H. D. Zhou, and S. E. Nagler, *arXiv:1204.2812v2*.

¹³The fourth structural phase transition from LT tetragonal to orthorhombic phase has been reported for a single crystal.¹¹ However, this further orthorhombic phase was not detected in other studies^{12,21} or in the present study. Therefore, only three phase transitions are shown in Fig. 1(b).

¹⁴S.-H. Lee, D. Louca, H. Ueda, S. Park, T. J. Sato, M. Isobe, Y. Ueda, S. Rosenkranz, P. Zschack, J. Iñiguez, Y. Qiu, and R. Osborn, *Phys. Rev. Lett.* **93**, 156407 (2004).

¹⁵E. M. Wheeler, B. Lake, A. T. M. Nazmul Islam, M. Reehuis, P. Steffens, T. Guidi, and A. H. Hill, *Phys. Rev. B* **82**, 140406(R) (2010).

¹⁶Y. Ueda, N. Fujiwara, and H. Yasuoka, *J. Phys. Soc. Jpn.* **66**, 778 (1997).

¹⁷H. Mamiya, M. Onoda, T. Furubayashi, J. Tang, and I. Nakatani, *J. Appl. Phys.* **81**, 5289 (1997).

¹⁸A. Kismarhadja, J. S. Brooks, A. Kiswandhi, K. Matsubayashi, R. Yamanaka, Y. Uwatoko, J. Whalen, T. Siegrist, and H. D. Zhou, *Phys. Rev. Lett.* **106**, 056602 (2011).

¹⁹S. Ohtani, Y. Watanabe, M. Saito, N. Abe, K. Taniguchi, H. Sagayama, T. Arima, M. Watanabe, and Y. Noda, *J. Phys.: Condens. Matter* **22**, 176003 (2010).

²⁰M. J. Harris, S. T. Bramwell, D. F. McMorrow, T. Zeiske, and K. W. Godfrey, *Phys. Rev. Lett.* **79**, 2554 (1997).

²¹S. Sarkar and T. Saha-Dasgupta, *Phys. Rev. B* **84**, 235112 (2011).

²²J. Kanamori, *J. Appl. Phys.* **31**, S14 (1960).

²³D. Okuyama, Y. Tokunaga, R. Kumai, Y. Taguchi, T. Arima, and Y. Tokura, *Phys. Rev. B* **80**, 064402 (2009).

²⁴Ü. Öpik and M. H. L. Pryce, *Proc. R. Soc. London Ser. A* **238**, 425 (1957).

²⁵J.-S. Kang, J. Hwang, D. H. Kim, E. Lee, W. C. Kim, C. S. Kim, S. Kwon, S. Lee, J.-Y. Kim, T. Ueno, M. Sawada, B. Kim, B. H. Kim, and B. I. Min, *Phys. Rev. B* **85**, 165136 (2012).